

Journal of Materials Chemistry B

Accepted Manuscript



This is an *Accepted Manuscript*, which has been through the Royal Society of Chemistry peer review process and has been accepted for publication.

Accepted Manuscripts are published online shortly after acceptance, before technical editing, formatting and proof reading. Using this free service, authors can make their results available to the community, in citable form, before we publish the edited article. We will replace this *Accepted Manuscript* with the edited and formatted *Advance Article* as soon as it is available.

You can find more information about *Accepted Manuscripts* in the [Information for Authors](#).

Please note that technical editing may introduce minor changes to the text and/or graphics, which may alter content. The journal's standard [Terms & Conditions](#) and the [Ethical guidelines](#) still apply. In no event shall the Royal Society of Chemistry be held responsible for any errors or omissions in this *Accepted Manuscript* or any consequences arising from the use of any information it contains.



Controllable synthesis of tetrapod gold nanocrystals with precisely tunable near-infrared plasmon resonance towards high efficient surface enhanced Raman spectroscopy bioimaging†

preReceived 00th January 20xx,
Accepted 00th January 20xx

DOI: 10.1039/x0xx00000x

www.rsc.org/

Jing Cai,^{ab} Vijay Raghavan,^b Yu Jie Bai,^c Ming Hui Zhou,^d Xiao Li Liu,^a Chun Yan Liao,^d Pei Ma,^a Lei Shi,^c Peter Dockery,^e Ivan Keogh,^f Hai Ming Fan,^{*ab} and Malini Olivo^{bg}

Tetrapod gold nanocrystals, to be the core of Surface-enhanced Raman spectroscopy (SERS) nanoprobes, with tunable localized surface plasmon resonance (LSPR) from 650 nm to 785 nm in Vis-NIR region have been successfully prepared by a facile seeded growth approach. The local electromagnetic field distribution and their huge extinction cross section of tetrapod gold nanocrystals were simulated by finite-difference time-domain method. Both the calculated and experimental results reveal that the LSPR property of tetrapod gold nanocrystals is closely dependent on the morphology features of their tips where strong field enhancement appears. These tetrapod nanocrystals have exhibited good capability not only for Raman signal enhancement but also successfully utilizing as NIR SERS bioimaging nanoprobes. In vitro SERS imaging of stained breast cancer cells has been also demonstrated. The tetrapod gold nanocrystals developed here with precisely tunable LSPR offer advantages of enhanced signal quality, good stability and better biocompatibility in SERS imaging, which has great potential for various biomedical applications.

1. Introduction

Recently, the applications of surface-enhanced Raman spectroscopy (SERS) in bioimaging have attracted much attention.¹ Due to the fact that the SERS nanoprobes have minimized photobleaching, multiplexing capability and high signal-to-noise ratio in complex biological systems compared with conventional fluorescent probes such as dyes and quantum dots, making SERS a great potential to be alternative to fluorescence-based bioimaging.² Up to now, Raman imaging using SERS nanoprobes has been demonstrated in various types of living cells,³ tissue⁴ and living animals.⁵ However, the intrinsic poor Raman signal leads to long acquisition time and low resolution, hindering their further application in bioimaging diagnostics.⁶ In addition, to avoid autofluorescence interfere and achieve deep tissue penetration, SERS measurements are required to be performed in the near-infrared (NIR) "bioimaging window".⁷ Therefore, the key challenge to realize clinically viable SERS labelled bioimaging hinges on the ability to design reliable and highly sensitive NIR SERS probes.

In general, SERS nanoprobes are constructed by attaching Raman active molecules (Raman reporter) to the surface of noble metal nanoparticles. According to the theoretical prediction, the SERS signal is strongly associated with the localized surface plasmon resonance (LSPR) property of noble metal nanoparticle.⁸ Along this line of thought, numerous studies have been devoted to the improvement of LSPR properties of noble metal nanoparticles and maximize its SERS signal. Gold nanoparticles are the most prevailing core used to construct SERS nanoprobes because of their excellent optical properties of surface plasmon resonance, the ease at chemical modification and good biocompatibility.⁹ Due to the rapid developments in synthetic chemistry, the methods of tailoring size and shape of Au core to acquire tunable SPR and enhanced SERS signal have been well-established.^{10,11} For instance, various structure gold nanoparticles such as nanospheres,^{2,12} nanorods,¹³ nanoclusters,¹⁴ nanoshells,¹⁵⁻¹⁷ as well as shell-isolated nanoparticles¹⁸ have been reported. Recently, a new class of gold nanoparticles, referred to as branched gold nanoparticles, has drawn much interests because their sharp tips can lead to strong localized electric field within single particle (so called lightning rod effect)¹⁹ and significant enhancement in Raman signal.²⁰⁻²³ For example, Yuan et al. had integrated branched gold nanoparticles with NIR resonant dyes to surface enhanced resonant Raman spectroscopy (SERRS) probes for Multiplexing detection.²⁴ Xie et al. synthesized branched gold nanoparticles by a seedless one-pot approach,²⁵ which had been further developed by Dam et al. for direct visualization of interactions between drug-loaded branched nanoparticles and cancer cell nucleus.²⁶ However,

^a School of Chemical Engineering, Northwest University, 229 Taibai Rd, Xi'an, Shannxi, 710069, P. R. China. Email: fanhm@nwu.edu.cn

^b School of Physics, National University of Ireland, Galway, Ireland.

^c Department of Physics, Fudan University, Shanghai 200433, P. R. China.

^d Department of Physics, Northwest University, Xi'an 710069, P. R. China.

^e Department of Anatomy, National University of Ireland, Galway, Ireland.

^f Department of Surgery, National University of Ireland, Galway, Ireland.

^g Singapore Bioimaging Consortium, Agency for Science Technology and Research, Singapore, 138667, Singapore

† Electronic Supplementary Information (ESI) available. See DOI: 10.1039/x0xx

the Au branched nanoparticles synthesized in most of studies have uncontrollable tip numbers and morphology, which in turn result in uncertain SPR characteristic. This has largely hindered the development of high efficient SERS nanoprobe using these branched nanoparticles. Furthermore, either silver ions or cetyltrimethylammonium bromide (CTAB) is commonly introduced in conventional synthetic approaches to promote the anisotropic growth of tips on gold nanoparticle, while they are toxic and difficult to be removed completely. Therefore, large-scale synthesis of the branched gold nanocrystals with shape-controllable tips and precisely tunable SPR in NIR region is strongly desirable.

In the present study, we prepared a series of tetrapod gold nanocrystals with tunable LSPR in NIR region by a facile seeded growth approach. The initial branched gold seeds are grown by a modified green chemical route. By elaborately adjusting the reaction condition, the shape of tips on the nanocrystals could be precisely controlled, leading to the continuous LSPR modulation from 650 nm to 785 nm. The finite-difference time-domain (FDTD) simulations reveal that the LSPR of the tetrapod gold nanocrystal is strongly associated with the sharpness and length of tips, which is consistent with experimental observation. These tetrapod nanocrystals have been further exploited to achieve NIR SERS nanoprobe for cellular Raman imaging. Raman measurements indicate that the tetrapod gold nanocrystals with LSPR of 770 nm can exhibit the strongest Raman signal enhancement under 785 nm laser. As prove of concept, *in vitro* SERS imaging using stained human breast cancer cells (SK-BR-3 cell line) has also demonstrated. This study aims to develop a facile method to controllable synthesis of tetrapod gold nanocrystals for various SERS bioimaging applications.

2. Experimental section

2.1. Preparation of tetrapod Au nanocrystals

All chemicals were purchased from Sigma-Aldrich and used as received. The glassware was cleaned with Aqua Regia (HCl/HNO₃ in 3:1 ratio by volume) and rinsed with deionized (DI) water. The samples are labeled by their extinction peaks of LSPR such as Au₆₇₀ and Au₇₇₀. In a typical experiment of tetrapod Au₆₇₀ nanocrystals, 4-(2-Hydroxyethyl)-1-piperazine propanesulfonic acid (EPPS) with a concentration of 100 mM was prepared and the pH of EPPS solution was adjusted to ~7.4 by adding with 1 M NaOH solution at room temperature. Then 9 mL EPPS was mixed with 10 mL of Deionization (DI) water, and followed by the addition of 150 μ L of 20 mM HAuCl₄ solution. After 120 min standing without any shaking, the color of solution changed from light yellow, pinkish purple to greenish blue in 120 min, indicating the formation of tetrapod Au₆₇₀ nanocrystals. By adjusting the amount of EPPS volume, the Au₆₂₀ and Au₆₄₀ nanocrystals were obtained. The tetrapod Au₆₉₀ nanocrystals were prepared by adding extra 50 μ L of 20 mM HAuCl₄ solution into initial reaction solution of tetrapod Au₆₇₀ nanocrystals under magnetic stirring at 35 °C for 60 min, where the as-prepared Au₆₇₀ nanocrystals were

used as seeds. Following the same procedure, the Au₇₁₀-Au₇₈₅ tetrapod nanocrystals were obtained in sequence. All samples were centrifugal separation and rinsed thrice with DI water, and then stored at 4 °C fridge for future use.

2.2. Preparation of SERS nanoprobe

In typical experiment, 166.6 μ L of 3, 3'-diethylthiatricarbocyanine iodide (DTTCi) with various concentrations from 1 μ M to 6 μ M were added into 1 mL tetrapod Au nanocrystals colloidal solutions (0.2 mM) and mixed by ultrasonication for 10 min. The optimized concentration of DTTCi was achieved by estimating maximal SERS intensity. Then, the methoxy poly(ethylene glycol) sulfhydryl (HS-mPEG, MW 5000) solution (100 μ M) was added dropwise to the each Au colloidal solution with a minimum ratio of 30,000 HS-mPEG molecules per tetrapod Au nanocrystals. The mixture was then shaken for 2 h under ambient conditions. Unbound DTTCi and HS-mPEG were removed by centrifugation. The obtained SERS nanoprobe were rinsed twice with DI water and stored at 4 °C for further use.

2.3. Material characterizations

The size and morphology of tetrapod Au nanocrystals were examined by a transmission electron microscope (TEM, JEOL JEM-1010). Extinction spectra were taken using a UV-2401 spectrometer (Shimadzu, Kyoto, Japan). Dynamic light scattering (DLS) measurements were performed using a Malvern Zetasizer Nano-ZS (Malvern Instruments, Worcester-shire, UK). Raman measurements were conducted by WITec Alpha-500 Raman microscope system with a 785 nm laser excitation source. A 60 \times objective lens with long working distance was used.

2.4. Cellular SERS measurements

SK-BR-3 human breast cancer cells purchased from ATCC (USA) were cultured in McCoy's 5A medium supplemented with 10% (v/v) fetal bovine serum (FBS) at 37 °C in a humidified atmosphere containing 5% CO₂. Cells in log growing phase were used for all experiments. SK-BR-3 cells were seeded and grown in 12-well plates, and incubated with SERS nanoprobe at concentrations of 450 pM for 4h at 37 °C. Untreated wells were used as control. Following incubation, the medium was removed and gently scrapped and resuspended in fresh cold PBS at the cell density of 10⁶ cells/cm³ for cellular SERS measurements.

2.5. *In vitro* cytotoxicity

The cell viability was determined by using 3-[4,5-dimethylthiazol-2-yl]-2,5-diphenyltetrazolium bromide (MTT) assay. The cells were seeded at a density of 12-well culture plates and incubated overnight at 37 °C with 5% CO₂. SERS nanoprobe with the different concentrations were added to the medium, and incubated with the cells in 5% CO₂ at 37 °C for 24 h in the dark. The suspension culture medium was removed and replaced by MTT solution followed by incubation for 4 h at 37 °C, allowing formazan purple crystals formation. The optical density at 540 nm was measured by using ELISA reader.

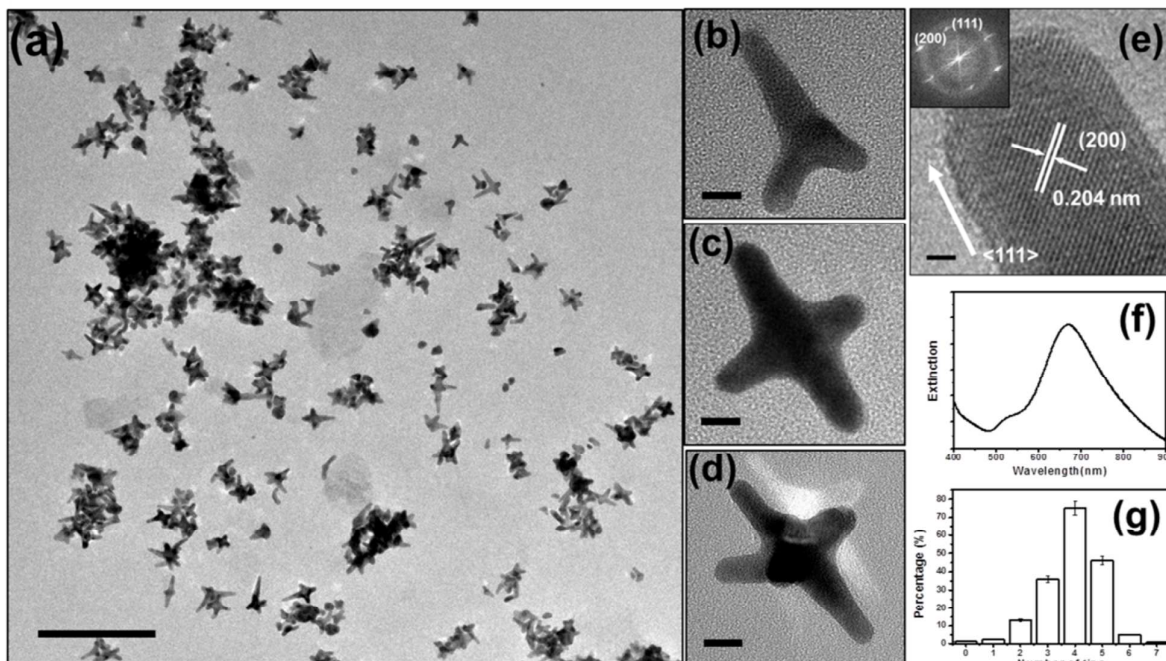


Fig. 1 (a) TEM images of the tetrapod Au nanocrystals. The scale bar is 200 nm. (b-d) TEM images of single tetrapod Au nanocrystal. The scale bars are 10 nm. (e) The HRTEM image of a tip, where the $\langle 111 \rangle$ growth direction of the tip can be clearly identified. The scale bar is 1 nm. The inset is corresponding FFT pattern. (f) Typical extinction spectrum of tetrapod Au nanocrystals. (g) Yield of Au nanocrystals as a function of the number of tips.

3. Results and discussion

Branched Au nanocrystals have been demonstrated to act as potential SERS nanoprobe because its unique optical properties could provide much more “hot spots” within a single particle. Branched Au nanocrystals are usually prepared by either seed-mediated or seedless growth, where surfactant molecules such as CTAB,²⁷ poly(vinylpyrrolidone) (PVP),²⁸ 2-[4-(2-Hydroxyethyl)-1-piperazinyl] ethanesulfonic acid (HEPES)²⁵ are used to realize the kinetically controlled anisotropic growth. In this work, branched Au seeds were grown initially by a modified solution growth approach, where EPPS is used to replace HEPES as both reducing and shape-directing agent. Similar to HEPES, EPPS is also a common Good’s buffer used in chemistry and biochemistry laboratories. However, EPPS with additional $-\text{CH}_2-$ group between the piperazine ring and the sulfonic acid group can reduce the reaction rate and facilitate controlled growth of branched Au nanoparticles in a reliable and reproducible way.²⁹ The comparison of reaction rate for EPPS and HEPES has been shown in Fig. S1. Fig. 1(a) shows the TEM image of initially branched Au seeds (Au_{670}) prepared using EPPS. It can be seen that the branched Au nanocrystals are synthesized in a large scale, while the tetrapod Au nanocrystals are the majority nanostructures (75%) identified under the TEM observation (Fig. 1g). The Au nanocrystals have the average size of ~ 40 nm. Fig. 1b-d shows the TEM images of typical Au nanocrystals with three, four and five tips. The

lengths of the branches are from 16 to 18 nm. High resolution TEM images and corresponding fast Fourier transform (FFT) analysis as shown in Fig. 1e reveals that the growth direction of the tip is along $\langle 111 \rangle$, consistent with the previous report.²⁵ Between the two adjacent planes on tips, the lattice spacing is

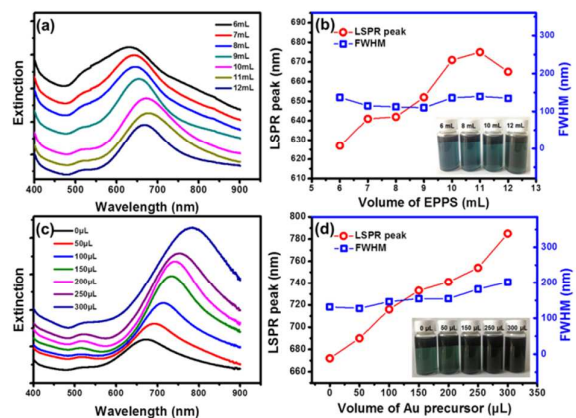


Fig. 2 (a) Extinction spectra of the Au nanocrystals obtained with the varied EPPS volume. (b) The LSPR peaks and their FWHMs of the Au nanocrystals as a function of the EPPS volume. Inset is the photograph of the Au nanocrystals aqueous solutions obtained by varying EPPS volume. (c) Extinction spectra of tetrapod Au nanocrystals obtained by adding extra Au precursors gradually (50 μL for each step). (d) The LSPR peaks and their FWHMs of the Au nanocrystals as a function of Au precursor volume. Inset is the photograph of the Au nanocrystals aqueous solutions obtained by adding extra Au precursors.

found to be 0.204 nm that is in agreement with the *d* spacing of the (200) lattice planes. The extinction spectrum of as-prepared tetrapod Au nanocrystals is presented in Fig. 1f. A strong extinction peak at 670 nm and a weak shoulder at ~520 nm are observed, which are derived from the hybridization of tips and core plasma.³⁰

We further investigate the effect of reaction parameters such as pH, temperature, the concentration of Au precursors and EPPS on LSPR property of branched Au seeds. It is well known that the shapes of Au nanoparticles have significant impact on their LSPR properties, the modulation of the reaction parameters could kinetically control the growth of Au nanocrystals and may result in different shapes and varied LSPR.³¹ The growth process of branched Au seeds has been monitored by time-course measurements of extinction spectra (Fig. S2a). The morphology evolution is observed by TEM (Fig. S2c-e). The results reveal that the tiny gold nanocrystals are initially formed and subsequently the branches appear on the nanocrystals. The further anisotropic growth with the help of EPPS leads to the sharp tips of tetrapod Au nanocrystals. Fig. 2a shows the extinction spectra of Au nanocrystals obtained at different EPPS volume. It is clear that LSPR peak of Au nanocrystals is red-shifted with the increasing volume of EPPS from 6 to 11 mL. Further increasing the EPPS volume to 12 mL will lead to blue shift of LSPR. In addition, at the EPPS volume smaller than 6 mL, the morphology of nanocrystals transform

from tetrapod to two-tip nanocrystals (Fig. 4a). Fig. 2b depicts the LSPR dependence of EPPS volume and the inset shows the photographs of obtained Au nanocrystals. The LSPR peak is gradually shifted from gradually from 620 nm to 670 nm and the variation of the full width at half maximum (FWHM) are relatively small (around 20 nm). The narrow FWHM indicates good uniformity of Au nanocrystals obtained by this modified solution methods.³² The modulations of other reaction parameters are presented in Fig. S3. As shown in Fig. S3a, the Au₆₇₀ nanocrystals can be well reproduced at the temperature between 4 and 35 °C, while only a slight red-shift is found with the increasing temperature. However, a sharp blue-shift of LSPR to 605 nm appears at the temperature of 40 °C, indicating that the significant morphology change happens in Au nanocrystals at high temperature. Similarly, increasing the Au precursors will also lead to enhanced reaction rate and blue-shift in LSPR as shown in Fig. S3b. With the pH value adjusting from 6 to 9, the corresponding characteristic peak of LSPR is red-shifted from 635 to 690 nm, but blue-shifted to 630 nm when pH value over 9.6 (Fig. S3c). Since high pH value promote the Au reduction reaction, this sudden blue-shift of LSPR obviously can also be attributed to faster reaction rate at high pH value. The results reveal that the adjusting of EPPS concentration presents a straightforward and feasible approach to modulate LSPR of tetrapod Au nanocrystals. Nevertheless, the LSPRs modulated by this way are limited in

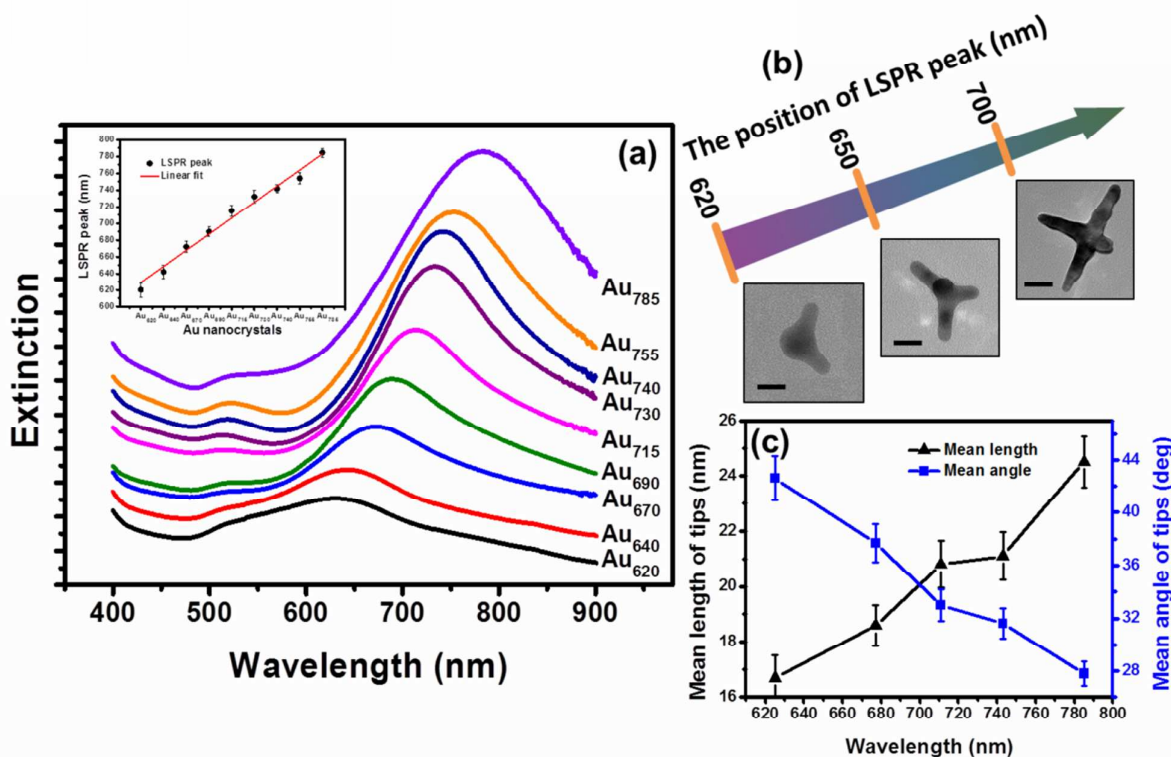


Fig. 3 (a) Extinction spectra of Au nanocrystals with tunable LSPR peaks. The inset illustrates that LSPR peaks of the Au nanocrystals can be linear modulation in NIR region. (b) Schematic illustration of the morphology evolution of the Au nanocrystals with different LSPR peaks. The scale bars are 20 nm. (c) The mean length and apex angle of the tips on the tetrapod Au nanocrystals as a function of LSPR peak.

the range from 620 to 670 nm and the morphology of tetrapod Au nanocrystals is also changed to two-tip structure at certain condition.

In order to further tune LSPR of tetrapod Au nanocrystals to longer wavelength without any change in morphology, a seeded growth process was employed. To avoid self-nucleation at high Au precursor concentration, small amount of Au precursors (tetrapod Au₆₇₀ nanocrystals, 50 μ L) was added each time under magnetic stirring at 35 $^{\circ}$ C. Fig. 2c shows the extinction spectra of tetrapod Au nanocrystals obtained by seeded growth. As shown in Fig. 2d, LSPR peak of the tetrapod Au nanocrystals increases gradually from 670 to 785 nm by adding extra Au precursors. However, when the amount of Au precursors are greater than 300 μ L, LSPR peak of obtained Au nanocrystals appear blue-shift and broadening, and the morphology of Au nanocrystals become uncontrolled (Fig. S4). Fig. 2d shows LSPR peaks versus net additional amount of Au precursors. The LSPR peak shift around 20-35 nm step by step and at the same time the FWHM slightly increases from 125 to 200 nm. Insets of Fig. 2d shows the photographs of tetrapod Au nanocrystals obtained by seeded growth, in which the colour of Au nanocrystals are changed from blue to bluish green and dark bluish green as LSPR varies from 670 to 785 nm. The extinction spectra of all branched Au nanocrystals from Au₆₂₀ to Au₇₈₅ obtained in this work are shown in Fig. 3a and the LSPR peaks of the samples can be well fitted by linear curve (inset of Fig. 3a). To better understand the LSPR dependence of the shape of the nanocrystals, TEM investigations have been conducted. Fig. 3b shows the typical morphology of the nanocrystals in specific LSPR range. According to the TEM analyses, the prevailing morphology of the Au nanocrystals with LSPR peak below 650 nm is mainly two-tip structure. The tetrapod Au nanocrystals become dominant when LSPR peak greater than 650 nm. The mean length and angle of curvature of the tips for these tetrapod nanocrystals are plotted in Fig. 3c. The tips become longer and sharper with the LSPR peak shifting to longer wavelength because newly added Au precursors are likely to be reduced and deposit on the top of the tip due to its high reactivity. The effect of different Au seeds on the growth of tetrapod Au nanocrystals was also investigated. Fig. 4 shows the TEM images of different Au seeds and the branched Au nanocrystals prepared by seeded growth. The Au₆₂₀ seeds with the two-tip morphology (Fig. 4a) result in the branched Au nanocrystals with many short tips (Fig. 4c). While Au₆₇₀ seeds are typical tetrapod nanocrystals, their products maintain the tetrapod structure but elongate tips (Fig. 4b, 4d). The fine tuning of LSPR properties by this approach exhibit some merits that is distinct different from those obtained by direct adjusting the concentration of the reducing/surfactant molecules.³³ First, the red-shift of LSPR is almost linear in the range of 670 to 785 nm. Therefore, theoretically we can prepare the tetrapod nanocrystals with designed LSPR in NIR range. Second, the FWHMs of characteristic peaks do not have obvious broadening. In contrast, the broadening of peak has been observed for the tetrapod Au nanocrystals obtained by directly growth using HEPES.³² The results explicitly indicate that the

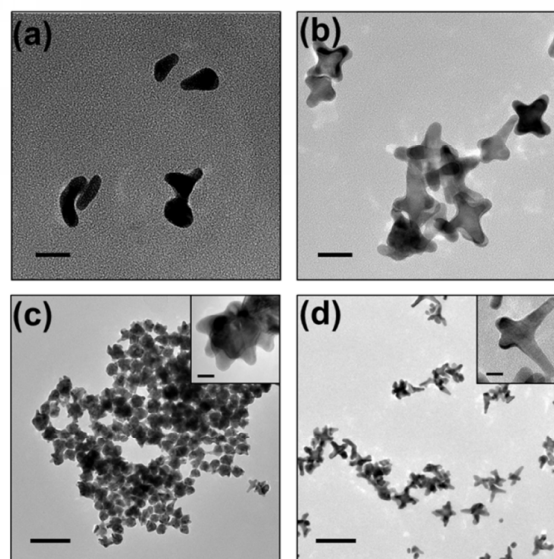


Fig. 4 TEM images of Au nanocrystals seeds with LSPR peak at (a) 620 nm and (b) 670 nm. The scale bars are 20 nm. (c, d) TEM images of Au nanocrystals after further growth with seeds (a) and (b), respectively. The scale bars are 100 nm in (c, d) and 10 nm in the inset.

seeded growth process provide a rational and dividable approach to realize precise tuning of LSPR.

The extinction properties of tetrapod Au nanocrystals and the correlation of LSPR and geometric features of tips on nanocrystals have been calculated and analysed by the FDTD simulation. We designed a tetrapod nanocrystal structure composed of a 7 nm spherical core and uniform tips with varied lengths L , apex angles θ and the angle α of the vertex tip in Z direction and other three tips (Fig. 5c). The excitation light is along the X direction. Without loss universality, there are four tips along X, Y and Z directions, which could present the most typical cases of the tip orientation under a linear polarized light. Fig. 5a shows the extinction spectra of tetrapod Au nanocrystals with the length from 12 to 30 nm and the apex angle of 45 $^{\circ}$, 36 $^{\circ}$ and 27 $^{\circ}$, respectively. It is evident that the LSPR peak is shifted to the longer wavelength with both increasing length and decreasing apex angle of tips. At each fixed θ , the LSPR will be shifted fast at short length region but slow down with the increasing length. The effect of the dipole interaction between the tips on LSPR of the nanocrystals is also investigated. We varied the angle α only and simulated the extinction spectra of tetrapod Au nanocrystals with varied angles. As shown in Fig. 5b, the LSPR peaks show small blue-shift from 715 nm to 695 nm as the angle α increase from 90 $^{\circ}$ to 150 $^{\circ}$, while the intensities are obviously reduced possibly due to the weakening of dipole interaction. Field distributions of a tetrapod nanocrystal with θ of 36 $^{\circ}$ are shown in Fig. 5d-f. The intensities of induced electromagnetic fields around the tips surface are quite strong, consistent with the previous studies.³⁴ The maximum field intensity approaches to the tip surface along X direction, which is parallel to the polarization direction of excitation electronic field.³⁵ These simulation

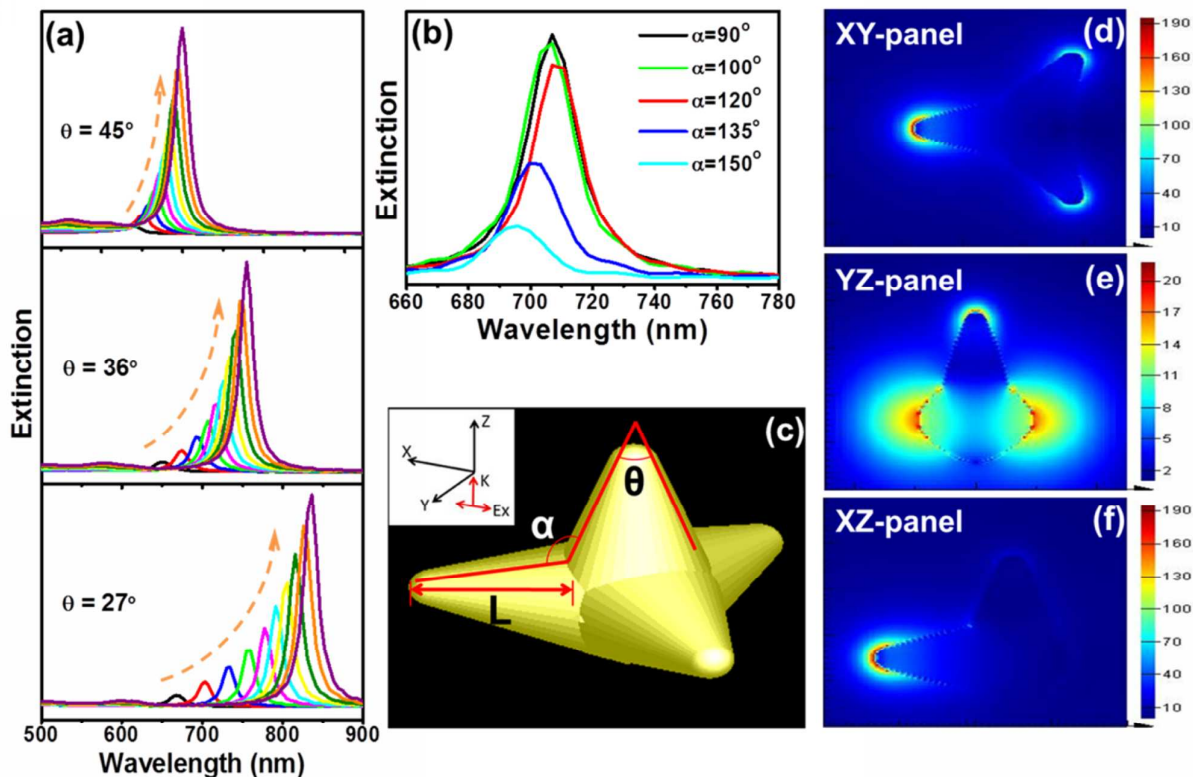


Fig. 5 (a) Simulated extinction spectra of a tetrapod Au nanocrystal with tuning geometric parameter tips. The lengths L of the tetrapod Au nanocrystal from left to right are 12 nm (black line), 14 nm (red line), 16 nm (blue line), 18 nm (green line), 20 nm (magenta line), 22 nm (cyan line), 24 nm (yellow line), 26 nm (olive line), 28 nm (orange line) and 30 nm (purple line), respectively. (b) Simulated extinction spectra of a tetrapod Au nanocrystal with tuning the angle α . (c) The model of a tetrapod Au nanocrystal for simulation. L is the length of tip. θ is the angle of the tip. α is the angle of the vertex tip in Z direction and other three tips. (d-f) FDTD simulations of the electric field distribution in XY plane, XZ plane and YZ plane. The excitation detection is along the X axis.

results reveal that the LSPR for a certain tetrapod Au nanocrystals could be ideally modulated by adjusting the length and sharpness of their tips, which are in good agreement with our experimental observations. In addition, we also compare the extinction cross-section of tetrapod gold nanocrystals to that of nanosphere, nanorod and nanoshell at same mass (Fig. S5). The results indicate that both tetrapod nanocrystal and nanorod exhibit large extinction cross-sections and thus a high theoretical SERS enhancement factors. However, the tetrapod gold nanocrystal has an optimal size between 50 and 100 nm for enhanced permeability and retention (EPR) effect and enhanced circulation time simultaneously.^{36, 37} In contrast the nanorods with the length of ~ 63 nm at the same mass, it may be more suitable as a NIR SERS probe for various biomedical applications. It is noted that this rough comparison may not be applicable for all cases because the intensity of SERS signal depends on many factors such as excitation laser, the type of Raman reporter, the type of metal nanoparticles, the shape of nanostructure and the distribution of local electric field as well as how many Raman reporter molecules locate in the area of hotspots etc.

To exploit the potential of tetrapod Au nanocrystals for high performance NIR SERS nanoprobes, we constructed the SERS nanoprobes by coating Raman reporter (DTTCi) and

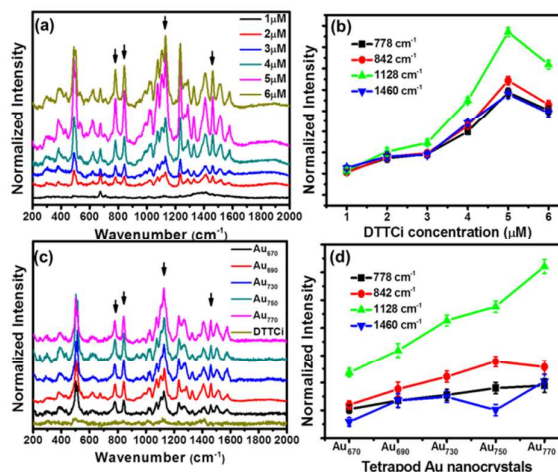


Fig. 6 (a) The Raman spectra of tetrapod Au nanoprobes prepared by using Au_{670} and varied DTTCi concentrations. (b) The normalized intensity of characteristic Raman peaks for the Au nanoprobes prepared by using Au_{670} and varied DTTCi concentrations. (c) The Raman spectra of tetrapod Au nanoprobes prepared by using different tetrapod Au nanocrystals and 5 μM DTTCi. (d) The normalized intensity of characteristic Raman peaks for the Au nanoprobes prepared by using different tetrapod Au nanocrystals.

stabilizer (HS-mPEG 5000) on tetrapod Au nanocrystals. The DTTCi molecules can bind to the surface of gold nanoparticles via N atom of pyrrol.³⁸ Fig. 6a shows the Raman spectra of SERS nanoprobe prepared by using Au₆₇₀ and different DTTCi concentrations under excitation (785 nm). The characteristic peaks are observed at 490, 640, 742, 778, 842, 984, 1029, 1076, 1128, 1233, 1277, 1328, 1409, 1460, 1511 and 1579 cm⁻¹, which can be indexed to the Raman vibrations of DTTCi molecules.³⁹ The Raman peaks of 640, 742, 778, 842 and 1277 cm⁻¹ are attributed to the stretching of carbon chain of DTTCi.⁴⁰ The Raman peaks of 984 and 1233 cm⁻¹ belong to CN stretching vibration. The Raman peaks of 490 and 1579 cm⁻¹ are assigned to CS stretching bending and CH torsion vibration, respectively. The Raman characteristic peaks of 1029, 1076, 1128, 1328, 1409, 1460, 1511 cm⁻¹ are belong to CC stretching vibration or bending.³⁸ Fig. 6b shows the normalized intensity of the Raman peaks at 778, 842, 1128 and 1460 cm⁻¹ with different DTTCi concentration. All peaks reach their maximums at a same concentration, suggesting that the optimized DTTCi concentration for SERS nanoprobe is 5 μM. The absorbed DTTCi estimated by optical density (OD) at 756 nm is about 10.60 mol/g Au (Fig. S6). Furthermore, we also compared the SERS spectra of the SERS nanoprobe prepared by using different tetrapod Au nanocrystals with absorbed DTTCi of 10.6±0.25 mol/g Au. The SERS spectra and the intensities of characteristic peaks at 778, 842, 1128 and 1460 cm⁻¹ are presented in Fig. 6c-d. It is clear that the Raman signal become much stronger when the LSPR peak is close to the 785 nm excitation line. Because the variation of absorbed DTTCi is quite small (<2.5%) the large Raman enhancement for Au₇₇₀ is possibly due to both resonance effect and enhanced local field.²⁴ The result indicates that the high performance NIR SERS nanoprobe could be constructed by using tetrapod Au nanocrystals with proper tuning LSPR.

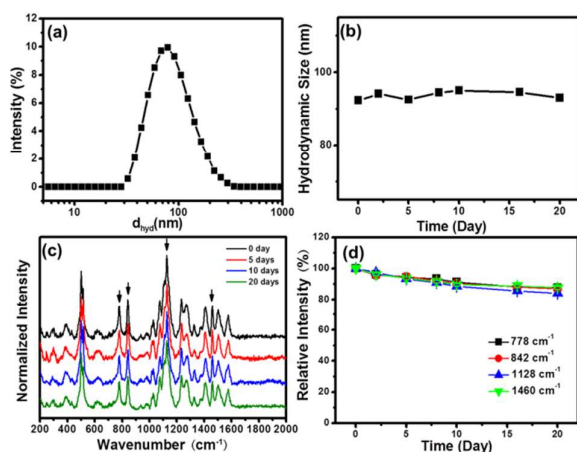


Fig. 7 (a) Hydrodynamic diameters of the Au₇₇₀ based SERS nanoprobe. (b) The colloidal stability test of the SERS nanoprobe. (c) The Raman spectra of the SERS nanoprobe stored for 0, 5, 10, 20 days, respectively. (d) The relative intensity of the Raman peaks for the SERS nanoprobe with different stored time.

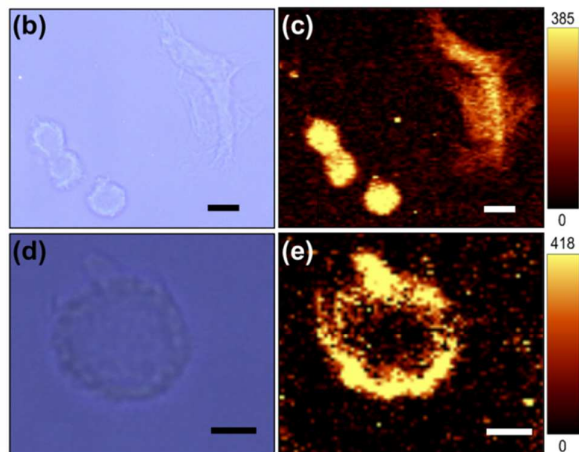
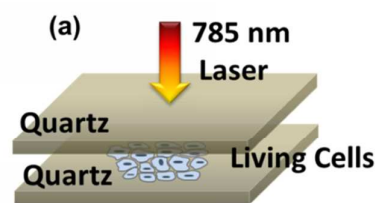


Fig. 8 (a) Illustration of experimental setup for Raman imaging. The optical image (b) and SERS image (c) of stained SK-BR-3 cancer cells. The scale bars are 10 μm in (b, c). The optical image (d) and SERS image (e) of single stained SK-BR-3 cancer cell. The scale bars are 5 μm in (d, e).

The colloidal stability and SERS signal stability of obtained SERS nanoprobe were examined using DLS and Raman measurements. The measured hydrodynamic size of Au₇₇₀ based SERS nanoprobe in aqueous solution is around 92.3 nm (Fig. 7a). The measured hydrodynamic sizes in aqueous solution are slightly larger than that of TEM observations due to the existence of the polymer coating on the nanoparticles. As shown in Fig. 7b, the hydrodynamic size of as-prepared SERS nanoprobe determined by DLS do not change significantly upon incubation in the water for 20 days, verifying the excellent colloidal stability of these SERS nanoprobe. Fig. 7c shows the Raman spectra of Au₇₇₀ based SERS nanoprobe after 5 to 20-day storage. The Raman spectra show insignificant change over a period of 20 days. As shown in Fig. 7d, the intensities of Raman peaks are retained over 80% after 20 days. The results from stability testing of SERS nanoprobe prove that the mPEG coated tetrapod Au nanocrystals possess good colloidal and SERS signal stability, therefore, such probes are suitable for in vitro/in vivo bioimaging applications.

The live-cell imaging based on the obtained SERS nanoprobe is further demonstrated using Witec confocal Raman system. The SK-BR-3 cells was used and incubation with SERS nanoprobe for 4 hours at 37 °C. After incubation, the stained cells were rinsing with PBS thrice and then placed between two quartz slides for Raman mapping measurement. The samples were excited with a 785 nm laser with a focal spot of 1 μm using 50 mW laser (Fig. 8a), and the intensity mapping measurements at 1460 cm⁻¹ were carried out as raster scans in 0.5 μm steps over the specified area (approx. 60×60 μm²) with

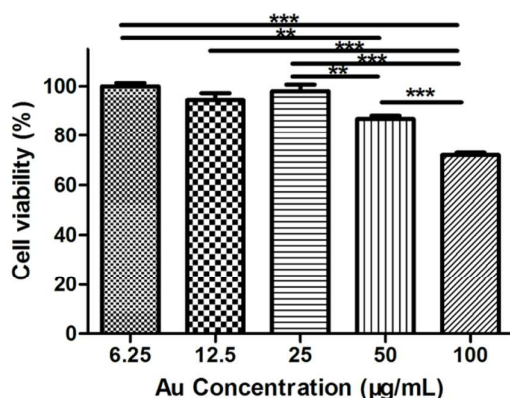


Fig. 9 Cell viability of Au₇₇₀ based SERS nanoprobe. Error bars represent mean \pm SD (n=3). *p < 0.05; **p < 0.01; ***p < 0.001.

1 s as the integration time per step. Fig. 8b-c show the bright-field image and Raman image of the stained cells, respectively. The Raman image is closely correlated with the bright-field image. An enlarged Raman image of single cell is presented in Fig. 8d-e. The image confirms the SERS nanoprobe are internalized into the cell and accumulated around cell nucleus. The results clearly indicate that the obtained tetrapod Au nanocrystals could be used to construct high performance NIR SERS nanoprobe for cell imaging, and it is also potential for other biomedical application in which excellent LSPR property in NIR region is required.

Since cytotoxicity is an important issue for nanoparticle based bioimaging, in vitro cytotoxicity test thus carried out to evaluate the cytotoxic profiles of SERS nanoprobe using standard cytotoxicity tests. Fig. 9 shows the viability of SK-BR-3 human breast cancer cells after 24 h incubation with SERS nanoprobe at 37 °C. The tetrapod Au nanoprobe exhibit insignificant toxicity even at 50 µg/mL with a cell viability of ~86% which is comparable to other Au nanoparticles based nanoprobe.⁴¹

4. Conclusion

In summary, tetrapod Au nanocrystals with tunable LSPR in NIR region have been synthesized by a facile seeded growth approach. The presented method can achieve precise modulation of LSPR peaks of tetrapod Au nanocrystals from 650 nm to 785 nm by controlling the length and sharpness of the tips on the nanocrystals. FDTD simulation and experimental results consistently reveal that the both the sharpness and length of the tips of tetrapod Au nanocrystals contribute to the peak shift of LSPR as well as the enhancement of local electromagnetic fields. These tetrapod Au nanocrystals have further exploited as high performance NIR SERS nanoprobe by decorating NIR Raman-active DTTCi as Raman reporter and HS-mPEG as protective layer. Among them, Au₇₇₀ based SERS nanoprobe show the strongest Raman signal and has been successfully applied to SERS imaging of SK-BR-3 human breast cancer cells. Besides high

Raman signal in NIR region, these SERS nanoprobe also demonstrate high stability in both colloidal system and Raman signal as well as good biocompatibility, indicating their great potential for in vivo bioimaging application. Although this study describes the application of the tetrapod Au nanocrystals as NIR SERS nanoprobe for bioimaging, we believe that these tetrapod Au nanocrystals with controllable LSPR in NIR region could find broad applications in biotechnology and medicine.

Acknowledgements

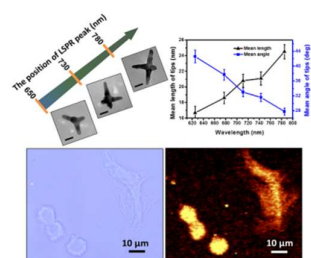
This work was financially supported by the National Natural Science Foundation of China (Grant No. 21376192, No. 11404064), the Science Foundation Ireland (Grant No. 10/IN.1/I2977), the Research Fund for the Doctoral Program of Higher Education China (Grant No. 20126101110017), the Program for Professor of Special Appointment (Eastern Scholar) at Shanghai Institutions of Higher Learning, Shanghai Pujiang Program (14PJ1401100).

Notes and references

- 1 T. Vo-Dinh, H.-N. Wang and J. Scaffidi, *Journal of Biophotonics*, 2010, **3**, 89-102.
- 2 X. Qian, X. H. Peng, D. O. Ansari, Q. Yin Goen, G. Z. Chen, D. M. Shin, L. Yang, A. N. Young, M. D. Wang and S. Nie, *Nat. Biotechnol.*, 2008, **26**, 83-90.
- 3 M. Potara, S. Boca, E. Licarete, A. Damert, M.-C. Alupeii, M. T. Chiriac, O. Popescu, U. Schmidt and S. Astilean, *Nanoscale*, 2013, **5**, 6013-6022.
- 4 M. Schütz, D. Steinigeweg, M. Salehi, K. Kömpe and S. Schlücker, *Chem. Commun.*, 2011, **47**, 4216-4218.
- 5 C. L. Zavaleta, B. R. Smith, I. Walton, W. Doering, G. Davis, B. Shojaei, M. J. Natan and S. S. Gambhir, *Proc. Natl. Acad. Sci. U. S. A.*, 2009, **106**, 13511-13516.
- 6 J. Qian, L. Jiang, F. Cai, D. Wang and S. He, *Biomaterials*, 2011, **32**, 1601-1610.
- 7 R. Weissleder, *Nat. Biotechnol.*, 2001, **19**, 316-316.
- 8 Y. Wang, B. Yan and L. Chen, *Chem. Rev.*, 2013, **113**, 1391-1428.
- 9 J. Z. Zhang, D. A. Wheeler, A. M. Schwartzberg and J. Shi, *Biomedical Spectroscopy and Imaging*, 2014, **3**, 121-159.
- 10 W. Jia, J. Li and L. Jiang, *ACS. Appl. Mater. Interfaces*, 2013, **5**, 6886-6892.
- 11 S. Barbosa, A. Agrawal, L. Rodriguez-Lorenzo, I. Pastoriza-Santos, R. A. Alvarez-Puebla, A. Kornowski, H. Weller and L. M. Liz-Marzan, *Langmuir*, 2010, **26**, 14943-14950.
- 12 P. N. Njoki, I. S. Lim, D. Mott, H. Y. Park, B. Khan, S. Mishra, R. Sujakumar, J. Luo and C. J. Zhong, *J. Phys. Chem. C*, 2007, **111**, 14664-14669.
- 13 L. Jiang, J. Qian, F. Cai and S. He, *Anal. Bioanal. Chem.*, 2011, **400**, 2793-2800.

- 14 G. B. Braun, S. J. Lee, T. Laurence, N. Fera, L. Fabris, G. C. Bazan, M. Moskovits and N. O. Reich, *J. Phys. Chem. C*, 2009, **113**, 13622-13629.
- 15 A. M. Gobin, M. H. Lee, N. J. Halas, W. D. James, R. A. Drezek and J. L. West, *Nano Lett.*, 2007, **7**, 1929-1934.
- 16 M. P. Melancon, W. Lu, Z. Yang, R. Zhang, Z. Cheng, A. M. Elliot, J. Stafford, T. Olson, J. Z. Zhang and C. Li, *Mol. Cancer Ther.*, 2008, **7**, 1730-1739.
- 17 A. Priyam, N. M. Idris and Y. Zhang, *J. Mater. Chem.*, 2012, **22**, 960-965.
- 18 J. F. Li, Y. F. Huang, Y. Ding, Z. L. Yang, S. B. Li, X. S. Zhou, F. R. Fan, W. Zhang, Z. Y. Zhou, Y. Wu De, B. Ren, Z. L. Wang and Z. Q. Tian, *Nature*, 2010, **464**, 392-395.
- 19 P. Liao and A. Wokaun, *J. Chem. Phys.*, 1982, **76**, 751-752.
- 20 J. Xie, Q. Zhang, J. Y. Lee and D. I. C. Wang, *ACS nano*, 2008, **2**, 2473-2480.
- 21 J. A. Webb, W. R. Erwin, H. F. Zarick, J. Aufrecht, H. W. Manning, M. J. Lang, C. L. Pint and R. Bardhan, *J. Phys. Chem. C*, 2014, **118**, 3696-3707.
- 22 L. Rodríguez-Lorenzo, R. A. Álvarez-Puebla, I. Pastoriza-Santos, S. Mazzucco, O. Stéphan, M. Kociak, L. M. Liz-Marzán and F. J. García de Abajo, *J. Am. Chem. Soc.*, 2009, **131**, 4616-4618.
- 23 E. S. Allgeyer, A. Pongan, M. Browne and M. D. Mason, *Nano Lett.*, 2009, **9**, 3816-3819.
- 24 H. Yuan, Y. Liu, A. M. Fales, Y. L. Li, J. Liu and T. Vo-Dinh, *Anal. Chem.*, 2013, **85**, 208-212.
- 25 J. Xie, J. Y. Lee and D. I. C. Wang, *Chem. Mater.*, 2007, **19**, 2823-2830.
- 26 D. H. M. Dam, J. H. Lee, P. N. Sisco, D. T. Co, M. Zhang, M. R. Wasielewski and T. W. Odom, *ACS nano*, 2012, **6**, 3318-3326.
- 27 T. K. Sau and C. J. Murphy, *J. Am. Chem. Soc.*, 2004, **126**, 8648-8649.
- 28 A. Kedia and P. Senthil Kumar, *J. Phys. Chem. C*, 2011, **116**, 1679-1686.
- 29 H. Liu, Y. Xu, Y. Qin, W. Sanderson, D. Crowley, C. H. Turner and Y. Bao, *J. Phys. Chem. C*, 2013, **117**, 17143-17150.
- 30 F. Hao, C. L. Nehl, J. H. Hafner and P. Nordlander, *Nano Lett.*, 2007, **7**, 729-732.
- 31 W. Ni, X. Kou, Z. Yang and J. Wang, *ACS Nano*, 2008, **2**, 677-686.
- 32 X. L. Liu, J. H. Wang, S. Liang, D. J. Yang, F. Nan, S. J. Ding, L. Zhou, Z. H. Hao and Q. Q. Wang, *J. Phys. Chem. C*, 2014, **118**, 9659-9664.
- 33 P. C. Angelomé, H. Heidari Mezerji, B. Goris, I. Pastoriza-Santos, J. Pérez-Juste, S. Bals and L. M. Liz-Marzán, *Chem. Mater.*, 2012, **24**, 1393-1399.
- 34 C. G. Khoury and T. Vo-Dinh, *J. Phys. Chem. C*, 2008, **112**, 18849-18859.
- 35 P. Das, A. Kedia, P. S. Kumar, N. Large and T. K. Chini, *Nanotechnology*, 2013, **24**, 405704.
- 36 H. Cabral, Y. Matsumoto, K. Mizuno, Q. Chen, M. Murakami, M. Kimura, Y. Terada, M. R. Kano, K. Miyazono, M. Uesaka, N. Nishiyama and K. Kataoka, *Nat Nano*, 2011, **6**, 815-823.
- 37 S. D. Perrault, C. Walkey, T. Jennings, H. C. Fischer and W. C. W. Chan, *Nano Lett.*, 2009, **9**, 1909-1915.
- 38 H. Cai, J. Zhu, G. Chen, L. Liu, G. S. He and X. Zhang, *J. Raman Spectrosc.*, 2011, **42**, 1722-1727.
- 39 F. Cai, J. Qian, L. Jiang and S. He, *Journal of biomedical optics*, 2011, **16**, 016002.
- 40 J. Casado, R. P. Ortiz, M. C. Ruiz Delgado, R. Azumi, R. T. Oakley, V. Hernández and J. T. López Navarrete, *J. Phys. Chem. B*, 2005, **109**, 10115-10125.
- 41 X. Liu, N. Huang, H. Wang, H. Li, Q. Jin and J. Ji, *Biomaterials*, 2013, **34**, 8370-8381.

Table of contents



Tetrapod gold nanocrystals have been controllably synthesized with tunable near-infrared plasmon resonance towards high efficient surface enhanced Raman spectroscopy bioimaging.